Theoretical Account of a Dry Sorption Injection Experiment

R. W. K. Allen, E. D. Archer, and J. M. MacInnes
The University of Sheffield, Dept. of Chemical & Process Engineering, Mappin Street, Sheffield, S1 3JD, UK

A theoretical representation of adsorption by particles injected into a gas stream that was developed previously is used to assess results from a dry sorption injection experiment. The particle-size distribution is required in the theoretical model, and this distribution is measured for the experimental particles. The pore-size distribution is also measured and used to determine particle properties, including the effective diffusivity in the pore passages within the particles, which is required by the model. Comparison of the model and experiment establishes the crucial importance of accurate knowledge of the equilibrium relation for the actual adsorbate–adsorbent system considered and of a reliable representation of particle size and shape.

Introduction

Pollutant emissions in gaseous streams are found in a wide range of industrial processes. The pollutant specie is often removed using a solid adsorbent material, commonly in the form of a packed bed of solid pellets. Packed beds have the drawback that at any one time only the particles within the adsorption front are actively adsorbing. The remaining particles in the bed are inactive, awaiting either the front to reach them or regeneration, yet all particles contribute to pressure loss across the bed at all times. Also, regeneration of a packed bed requires either a duplicate bed to allow alternation of regeneration and adsorption or a continuous recycling of particles, which is prone to difficulties.

A method that has been increasingly used is dry-sorbent injection, in which particles are introduced into the gas flow to be cleaned and collected at a downstream position after the adsorption has taken place. The conditions of dry-sorbent injection differ in several respects from packed-bed adsorption. The particles used are smaller in size, perhaps in the range 1 μm to 100 μm rather than millimeters as is typical of packed-bed pellets, so that they can remain suspended in the gas flow. Also, the particles in dry-sorption injection often possess a distribution of sizes as a result of the particle production method. Because the particles are small and are free to move with the gas, convective mass transfer is less important than in a packed bed where the particles are held in place and the gas flows by them.

Correspondence concerning this article should be addressed to J. M. MacInnes.

In the present work, the theoretical model developed previously by the authors (Allen et al., 2001) is applied to results from a dry-sorption injection pilot plant experiment. The model is based on the equation for mass conservation of the adsorbate specie in a spherical particle and the equation for adsorbate conservation in the bulk gas surrounding the particles, with account being taken of the particle-size distribution. Results of an experiment using the volatile organic compound perchloroethylene as adsorbate and commercially available activated carbon particles as adsorbent are used to assess the modeling. In the experiment, the bulk adsorbate gas concentration is measured at several positions along the flow in a pipe from the point of particle injection, so the particle uptake of adsorbate can be determined at various points in the adsorption process. Also, the particle-size distribution and the pore-size distribution within the particles are measured. These distributions allow the influence of particle size to be represented and the effective diffusivity of adsorbate within the particle pores to be determined. The equilibrium relation of the adsorbate–adsorbent system is derived from standard theory, although some modification to account for the presence of water and perhaps other influences is found to be necessary.

Experiment

The apparatus consists of a length of stainless-steel pipe with provision for introducing heated gas and adsorbate and

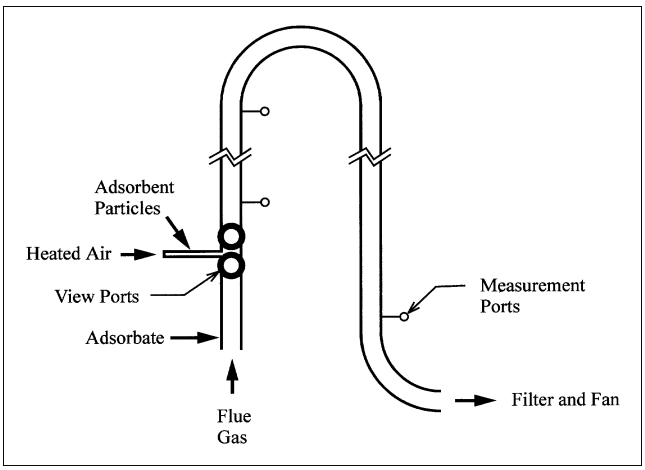

Figure 1. Experimental apparatus.

injecting particles under steady flow conditions. The experimental arrangement is shown in Figure 1. The pipe used has an 82.5-mm ID, d, and an overall length of about 7 m. This gives a maximum residence time of about 0.5 s for the design bulk velocity of 15 m/s. For the gas conditions used, the flow is fully turbulent ($Re_d = 45{,}200$). The flow is vertically upward for the first one-half of the pipe length, passes through a 180° pipe bend of radius ratio 6:1, and then continues downward in the vertical direction. The flow is driven by a downstream blower that is placed after a particle filter. The filter bags were automatically cleaned by reverse pulsed flow when filter pressure drop exceeded 20 Pa. The deviation in flow rate in the pipe associated with this changing filter pressure drop was estimated to be less than 2%. The pipe was lagged to maintain uniform gas temperature along the length. Thermocouple measurements at eight positions along the length confirmed that temperature varied by less than 6°C.

Flue gas from a natural gas boiler is used as the bulk gas stream with perchloroethylene (C_2Cl_4) as the adsorbate specie. The liquid adsorbate is injected into the flue-gas stream through a Biral 9302 atomizer, producing a gas stream at 150°C with an adsorbate mass fraction of 5.00×10^{-4}. Particles are introduced approximately 30 pipe diameters downstream of the adsorbate injection. The particles are conveyed in a stream of air, also at 150°C, to an injection nozzle. The nozzle introduces the air and particle flow through an oblong hole cut along the side of the nozzle tube, an area of about 47 mm^2. The nozzle directs the injection flow in the upstream (downward) direction and approximately parallel to the pipe axis. For the air flow rate used, the velocity at the nozzle exit is about 80 m/s. Table 1 gives a summary of flow rates and stream conditions of the experiment.

The particles used were activated carbon of type Fluesorb B supplied by Chemviron Carbon Ltd. These particles are produced by steam activation followed by grinding. Measurements of surface area and pore-size distribution were made as part of the experimental program to characterize the particles. A Micrometrics Gemini 2360 was used to measure the specific internal surface area of the particles, and the pore-size distribution was measured using a Micrometrics Pore Sizer 9320. The particle-size distribution was measured using a Particle Sizing Systems Accusizer 780A particle-sizing system.

Particle flow rates of 0.113, 0.43, 0.74 and 1.35 g/s were tested in the experiments. For each condition the initial adsorbate concentration and gas temperature remained the same. Concentration of adsorbate in the bulk gas was measured at three positions: 0.485, 3.435, and 6.505 m downstream of the particle injection nozzle exit. The concentration was measured using a flame ionization detector (Signal 3030PM Analyzer) with a sample extracted through a hole in the pipe side wall along a heated line. There is the possibility of further adsorption occurring during the delay time between extraction and the sample reaching the detector if particles pass through the sample line along with the gas. The line and particle filter in the line just before the detector were heated to a higher temperature (about 180°C) than that of the gas in the pipe, which countered this continuing adsorption by an opposing shift in the equilibrium. Readings produced using sample lines of 2 m and 0.5 m length gave the same concentration to within a few percent. The accuracy of the detector instrument itself is believed to be within about 5%.

Gas flow rates were measured using an orifice plate and a rotameter for the main gas flow and the injection gas flow, respectively. The gas density in each case was determined from temperature measurement using K-type thermocouples. The uncertainty of the flow-rate determinations is within a few percent. The mass flow rate of particles was determined by recording the change of weight in the particle hopper over the period of an experimental run at steady operation. The measured mass flow rate is reckoned to have an uncertainty of less than 1%. Thus, the uncertainties in determining the

Table 1. Experimental Conditions

	Flow Rates		Particle Characteristics
Total gas	67.2 g/s	ρ_P	624 kg/m^3
Gas injection	3.15 g/s	ϵ	0.672
Particle injection	0.113, 0.43, 0.74, 1.35 g/s	ϑ_e	3.47×10^{-6} m^2/s
	Gas Properties	τ	2
ρ	0.840 kg/m^3	K	985 kg/m^3
μ	2.30×10^{-5} Ns/m^2	q	0.337
ϑ	1.35×10^{-5} m^2/s	$\overline{D}_P$	20.1 μm
Y_{Bo}	5.00×10^{-4}	$\bar{s}$	1.01 μm
U	15.0 m/s	V	1.08×10^{-3} m^3/kg
d	0.0825 m	A	743×10^3 m^2/kg
$Re_d = \rho Ud/\mu$	45,200	A_{BET}	717×10^3 m^2/kg

flow rates and concentrations of adsorbate in the bulk gas are minor. The greatest uncertainty in the experiment, as will be seen, is in the determination of particle characteristics.

In the experiment considered, the collected particle mass is equal to the injected particle mass to within a few percent, and no deposit is apparent when the apparatus is dismantled. Thus, the fraction of injected particles that deposit on the walls of the apparatus is small and the process of deposition is not represented in the present modeling.

Model

The model developed previously by the authors (Allen et al., 2001) is used here to probe the experimental results. The model is based on the conservation equations for adsorbate in the pore gas within the particles, for the adsorbate in the bulk gas, and for particle mass. The distribution of particle size is represented in the model equations. The model makes the general approximations that particle properties are independent of particle size and uniform over the particle volume, that the particles are spherical, that gas properties within the pore are uniform (with the exception of adsorbate concentration), and that adsorption heating can be neglected. Many of these approximations follow directly from a restriction to low adsorbate concentration, which is the practical condition of usual applications of dry sorbate injection. The model is summarized here, but for a detailed discussion the reader is referred to Allen et al. (2001).

With the equilibrium between adsorbed mass per volume of particle, m, and gas-phase mass per volume, ρY, where ρ is gas density and Y is sorbate mass fraction in the gas, represented with the Freundlich relation,

$$m = K(\rho Y)^q, \tag{1}$$

the conservation equation for gas phase adsorbate at position r in a particle can be written in terms of particle porosity, ϵ, and adsorbate effective diffusivity, ϑ_e, as

$$\left[\epsilon + Kq(\rho Y)^{q-1}\right]\frac{\partial \rho Y}{\partial t} = \frac{1}{r^2}\frac{\partial}{\partial r}\left(r^2\epsilon\vartheta_e\frac{\partial \rho Y}{\partial r}\right). \tag{2}$$

This equation is solved for a spherical particle of diameter D_P, subject to the conditions of symmetry at the particle center and external adsorbate flux at the particle surface,

$$\epsilon\vartheta_e\frac{\partial \rho Y}{\partial r} = \rho h(Y_B - Y_S) \qquad \text{at} \quad r = \frac{D_P}{2}$$

$$\text{and} \quad \frac{\partial Y}{\partial r} = 0 \qquad \text{at} \quad r = 0, \tag{3}$$

and with zero mass of adsorbate within the particles at injection ($t = 0$). The mass-transfer coefficient, h, can be expressed in terms of the Reynolds number and the gas Schmidt number as

$$h = \frac{\vartheta}{D_P}(2 + 0.6Re^{1/2}Sc^{1/3}), \tag{4}$$

where

$$Re = \frac{\rho\,|\,u_P - U\,|\,D_P}{\mu} \quad \text{and} \quad Sc = \frac{\mu}{\rho\vartheta},$$

with U the average gas velocity in the pipe flow, u_P the particle velocity, and μ and ϑ the bulk gas viscosity and adsorbate diffusivity, respectively. Use of the mass-transfer coefficient in the external boundary conditions implies quasi-steady outer flow. The particle velocity appearing in the Reynolds number is determined from the Lagrangian equation of motion for the particle, which takes the form

$$\frac{du_P}{dt} = -g - \frac{(u_P - U)}{\tau_S}\left[1 + \frac{Re^{2/3}}{6}\right], \tag{5}$$

with the initial condition $u_P = 0$ at $t = 0$.

Allen et al. (2001) argue that the preceding equations simplify considerably depending on the values of parameters in the Freundlich equilibrium relation, gas properties, and particle pore effective diffusivity. It is found that, for large Biot number, $Bi = hD_P/\epsilon\vartheta_e$, just two parameters determine the adsorption by a particle: the exponent, q, in the equilibrium relation and the particle capacity parameter $K^*\phi_T$, where K^* is the nondimensional equilibrium adsorption coefficient defined as

$$K^* = \frac{Kq(\rho Y_{Bo})^{q-1}}{\epsilon} \tag{6}$$

and ϕ_T is the particle volume fraction when all sizes have reached mean equilibrium motion in the gas flow. The reduction of the particle adsorption process to dependence on just two parameters results from normalization of time by the usual diffusion time, D_P^2/ϑ_e, but also by the particle capacity K^* to give the nondimensional time variable t^*:

$$t^* = \frac{t\vartheta_e}{D_P^2(1 + K^*)}. \tag{7}$$

Four parameters affecting adsorption characteristics are summarized in Table 2, along with the values taken for the

Table 2. Experimental Parameters

$\frac{\text{Adsorption rate}}{\text{Accumulation rate}}$	K^*	8.5×10^4
$\frac{\text{External diffusion time scale}}{\text{Internal diffusion time scale}}$	$\frac{\vartheta}{\vartheta_e}\left[\frac{1}{K^*}\right]$	6.7×10^{-6}
$\frac{\text{Internal resistance to diffusion}}{\text{External resistance to diffusion}}$	$Bi = \frac{h\overline{D}_P}{\epsilon\vartheta_e} \approx \frac{2\vartheta}{\epsilon\vartheta_e}$	11
$\frac{\text{Stokes time scale}}{\text{Adsorption time scale}}$	$\left(\frac{\rho_P}{\rho}\right)\left(\frac{1}{1+K^*}\right)\left(\frac{\rho\vartheta_e}{\mu}\right)$	2.8×10^{-4}
$\frac{\text{Stokes time scale}}{\text{Flow time scale}}$	$\frac{\rho_p\overline{D}_P U}{18\,\mu L}$	1.1×10^{-3}

conditions of the present experiment. Adsorption coefficient K^* is large since, according to Lin et al. (1996), the adsorbate mass in the condensed (adsorbed) phase at equilibrium is invariably greater than that in the gas phase for the high pore surface-to-volume ratios of interest. With K^* large, the first term on the lefthand side of Eq. 2 becomes negligible; that is, accumulation of adsorbate in the gas in the particle pores is small compared with the adsorption rate. Also, the ratio of the time scale of response of the particle to changes in bulk gas motion (Stokes time scale) to the time scale of adsorption by the particle is small when K^* is large. For the experimental conditions here, this ratio of time scales is less than 10^{-3}. This means that Eq. 5 reduces approximately to $u_P = U$ during nearly the entire adsorption time. In terms of the time a particle spends in the pipe from injection to exit, the ratio of Stokes time to this residence time gives an indication of the initial fraction of the pipe length, L, where the velocities remain unequal. This fraction is about 10^{-3} in the present experiment, or only about the initial 7 mm of the flow. Finally, the ratio of time scales for external diffusion and internal diffusion (including the effect of adsorption within the pores) is less than 10^{-3}, so that the external diffusion process is quasi steady and it is possible to use a steady mass-transfer relation (Eq. 4) with good approximation.

Allen et al. (2001) estimated that "large" Biot number, for which adsorption is independent of either Reynolds number or Schmidt number, corresponded to Bi greater than about 40. For large Biot number, diffusion in the particle pores controls the rate of diffusion into the particle and there is no dependence on outer flow conditions. For the conditions of the present work, however, the Biot number is 11 and external mass transfer is significant. The extent of influence of the Biot number is shown in Figure 2, where the change in adsorbate uptake with time has been plotted. The Biot number has been varied by changing the free gas diffusivity, ϑ, with a 0.74 g/s mass flow rate of particles all of 20.1 μm and with all other parameters as in Table 1, that is, corresponding to the conditions of the present experiment. One can see that there is relatively little effect of external diffusion for Biot number greater than around 100. For $Bi = 11$, as in the present experiment, though, quite a large effect is present.

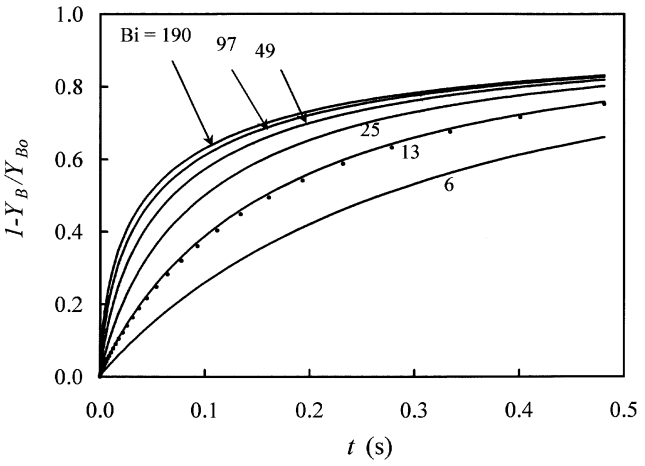

Figure 2. Effect of Biot number on adsorbate uptake.

Dots indicate the effect for $Bi = 13$ of excluding the representation of gas turbulence in the mass-transfer model.

The importance of external diffusion raises the question of the influence of turbulence in the flow. Mass transfer can be augmented by turbulent gas-velocity fluctuation that will contribute to the velocity difference between the particle and the gas in the Reynolds number of Eq. 4. An estimate of the average level of relative velocity associated with turbulent fluctuation may be derived from the result of Rizk and Elghobashi (1989), who examined the response of particles to a spectrum of fluid fluctuation and found the result

$$\frac{\overline{u_P'^2}}{\overline{u'^2}} = \left(1 + 5\frac{\tau_S}{\tau_T}\right)^{-1}, \tag{8}$$

with the Stokes time scale given by $\tau_S = \rho_P D_P^2/18\mu$, where ρ_P is the particle density, and the turbulent time scale by $\tau_T = k/\epsilon_k$, where k is the turbulence kinetic energy and ϵ_k its dissipation rate. Using the approximations $u' = \sqrt{\overline{u'^2}} = 0.07U$ and $\tau_T = 5D/U$, where D is the pipe diameter, as the average turbulence characteristics over a section of developed pipe flow, one finds the estimate for the additional relative velocity characteristic of the turbulent fluctuations

$$\frac{u_P' - u'}{U} = 0.07\left[1 - \frac{1}{\sqrt{1+St}}\right], \tag{9}$$

where St is the Stokes number, $St = \tau_S U/D$. The fluctuation relative velocity given by Eq. 9 has been included in the computations of this work. It has the greatest effect for the largest particles, since these have the largest Stokes number. However, the effect is minor, since the Reynolds number in Eq. 4 remains low even with the turbulence contribution. For the 20.1 μm particle with $Bi = 13$, the effect of not including the turbulence contribution of Eq. 9 is shown in Figure 2 as a series of dots. The shift from the solid curve is slight.

The bulk gas adsorbate concentration depends on the take-up of adsorbate by particles of different size. The bulk adsorbate mass fraction depends on the balance between convection and diffusion of adsorbate in the bulk gas and the rate of adsorbate transfer to the particles at any location in the flow. In the pipe flow considered here, it is a good approximation to neglect diffusion in the bulk gas as a mechanism affecting the bulk gas adsorbate concentration and to approximate the spatial change in bulk adsorbate along the pipe as the equivalent change with time following the flow. Introducing the volume fraction distribution function of particle size, f_V, and integrating over the adsorption rate $\dot{m}$ for a single particle of size D_P over all particle sizes to get the total adsorption, one can write the equation for bulk gas adsorbate mass per unit volume:

$$\frac{d\rho Y_B}{dt} = -\int_0^\infty \dot{m}\frac{\phi}{V_P} f_V \, dD_P, \tag{10}$$

where V_P is the volume of a particle of size D_P and ϕ is the volume fraction of particles in the particle–gas mixture. Time is measured from the point of injection and can be related to

distance along the pipe from the injection point by $x = Ut$. The particle volume fraction in the flow needs to be determined from the particle mass balance. For particle-size range dD_P about D_P, this can be written in terms of the injection particle-mass flow rate, $\dot{M}$, as

$$\phi f_V dD_P = \frac{\dot{M}}{\rho_P A u_P} f_{Vo}\, dD_P, \tag{11}$$

where A is the pipe cross-sectional area and f_{Vo} is the particle-size distribution of the particles in the static sample. In general, the distribution at any location in the flow is different because of the different velocities reached by particles of different size under the influence of gravity in the flow. Under the conditions of the experiment considered here, however, particles of all sizes move with a velocity that is close to that of the gas flow since the Stokes number is small. Integration of Eq. 11 over all particle sizes leads to an equation for the particle volume fraction in the flow,

$$\phi = \frac{\dot{M}}{\rho_P A} \int_0^\infty \frac{f_{Vo}}{u_P}\, dD_P. \tag{12}$$

It can be noted that with $u_P = U$ beyond the initial flow, as just shown, ϕ is a constant and equal to $\dot{M}/\rho_P UA$, and f_V is also constant and identical to the static distribution. In the computations with the model presented here, the full equations above are used. The numerical solution (Allen et al., 2001) involves a straightforward fully implicit finite volume scheme in which radial space is divided into 60 grid cells and particle diameter space is divided into 25 grid cells. However, before sensible computations of an experiment can be made with the model, reliable information about the particle-size distribution, the particle porosity and effective diffusivity and the coefficients in the equilibrium relation must be available. Determination of these model parameters is considered in the next several sections.

Particle Characterization

The model equations require that a number of physical characteristics of the particles are known for effective comparisons to be made. The particle porosity, density, and size distribution all must be known. Further, the pore-size distribution and structure that determine intraparticle diffusion are needed. A number of measurements have been undertaken as part of the experimental program and these are described here.

Pore-size data from two sources have been used. The particles are supplied with pore volume size distribution data from the manufacturer, resulting from a combination of mercury and nitrogen porosimetry. The volume distribution for large pore sizes—those accessible to the mercury porosimetry—were also measured in the present work for the actual particle samples used in the experiments. After discarding readings of large pore size judged to correspond to interparticle spaces in the test samples and using the manufacturer's information to account for the contribution of small pore volume, the two independent distributions could be compared directly, as shown in Figure 3. The two determinations are

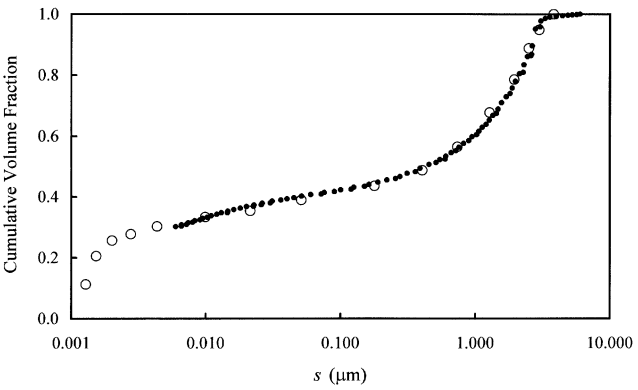

Figure 3. Cumulative volume distribution of pore size in the particles.

Open circles are data supplied by the manufacturer; filled circles are the present mercury porosimetry measurements.

clearly consistent and show that around 30% of the pore volume is undetected by the mercury porosimetry method alone.

From the measured pore-size distribution and the value of solid carbon density (taken as 1900 kg/m^3), the particle porosity, density, and pore volume per mass can be determined (Table 1). The pore-size data will be used further to estimate effective diffusivity within the particles. For this purpose details of pore structure, that is, the actual shape of the pore volume, would be useful. However, no information about structure is available, so the estimates will need to be based on some approximation.

The particles used in the study have been produced by steam activation followed by grinding, producing a collection of particles having a broad size distribution and nonspherical shape. Particle size is an important determining factor of the time scale of adsorption by a particle, with the time depending on the square of particle diameter (Eq. 7) for a spherical particle. Thus, it is crucial to have an accurate representation of particle-size distribution. The Accusizer was used to measure particles sampled from the pipe flow. The sampled particles were combined with liquid (containing a surfactant to reduce agglomeration) and the mixture passed through the detection volume. The particle-size distributions measured at injection and just before the filter indicated insignificant change to the particle distribution during passage through the pipe.

Several aspects of the particle-size measurement method tend to overestimate the particle size. These include the simultaneous arrival of two particles in the detection zone, causing undercounting of small particle volume, and counting of two or more smaller particles together in the detection zone as though they are a single larger particle. Each of these should introduce negligible error at the levels of particle-sample dilution used. Even though a surfactant was used, some agglomeration still occurred. It is thought that this agglomeration may have distorted the size distribution by an amount corresponding to a mean particle-size change of a few percent. The measured particle-size distribution is shown in Figure 4. The volume average size for the measured distribution is 20.1 μm, but significant volume is found below 5 μm and above 60 μm. This range of particle size corresponds to over a factor of 100 in particle adsorption time scale.

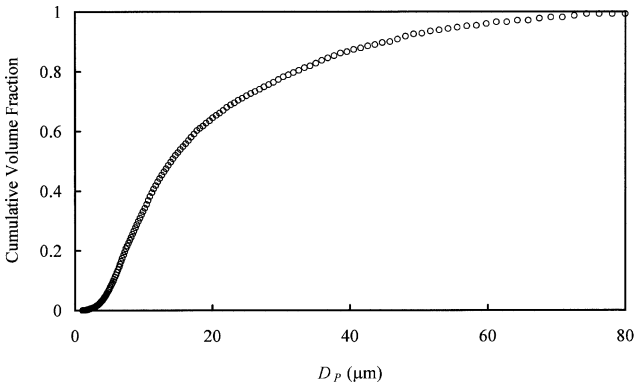

Figure 4. Measured cumulative volume distribution of particle size.

The possibility of particle agglomeration under the conditions of the experiment must also be considered. First of all, the large aerodynamic forces on particles as they flow through the injector nozzle should break up any agglomerated particles as they are introduced into the pipe flow. During passage along the pipe, estimates of particle collision rates for the conditions of the experiment (Archer, 2000) indicate that subsequent reagglomeration can be neglected.

The size instrument detects particle projected area and reports a particle size equal to the diameter of the sphere having the same projected area. Figure 5 shows a microphotograph of a sample of particles from the experiment, and these are certainly nonspherical. Nonspherical particles will be assigned a diameter in the measurement method that is larger than the characteristic distance for diffusion across the particle. A further concern with regard to particle shape is the use of spherical particles in the model formulation. The strategy being implicitly adopted is to avoid solving three-dimensional equations for the intraparticle diffusion process. It is likely that the use of an effective diffusion diameter will give an adequate account of nonspherical particle shape, and this requires particle-shape measurement as part of size characterization. Kaye (1999) gives an account of developments in this area.

Effective Diffusivity

The measured characteristics of the pores are now used to determine the effective diffusivity, ϑ_e, appearing in the model equations. The effective diffusivity depends on the pore size

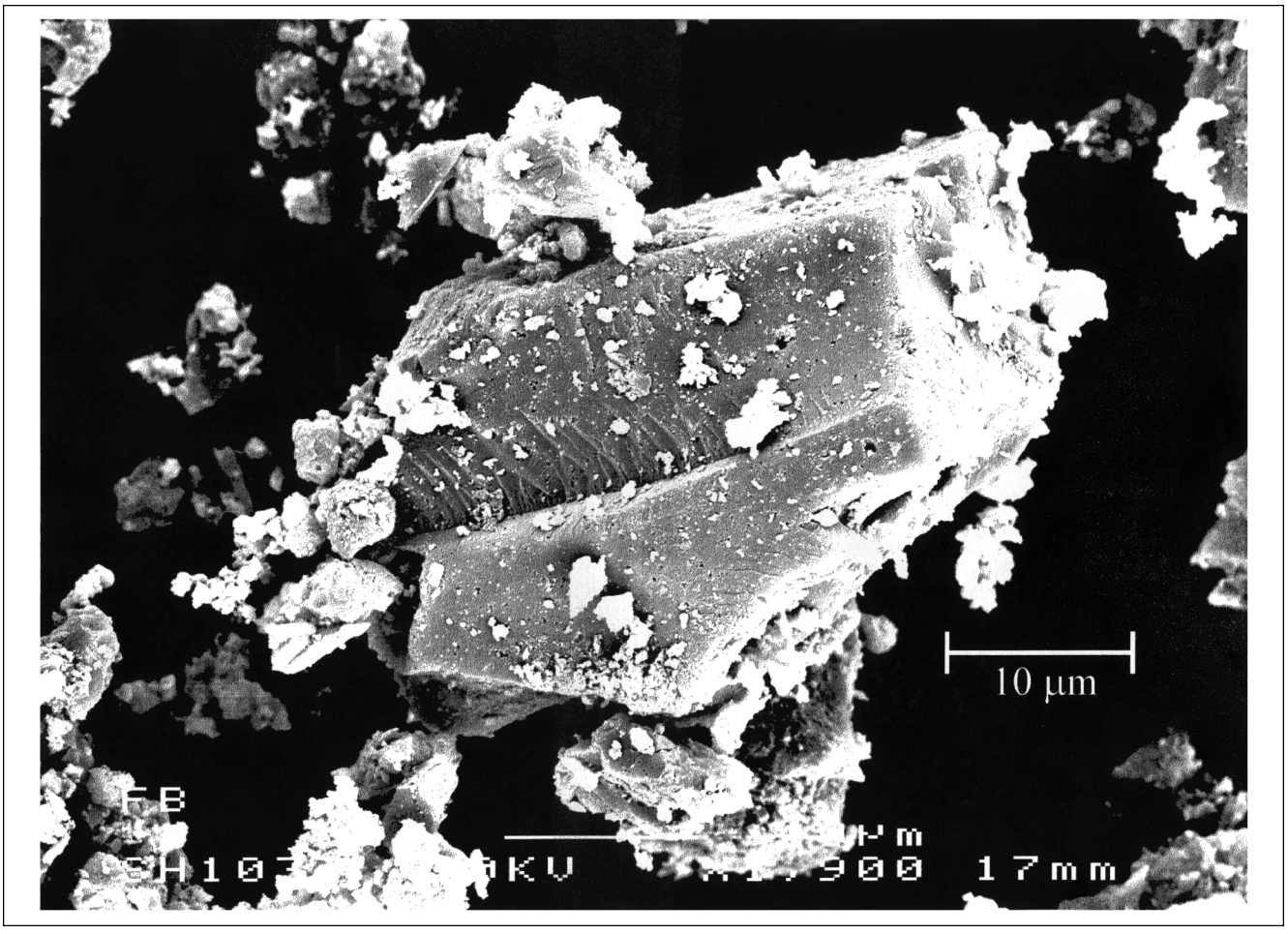

Figure 5. Electron microscope image of a sample group of particles.

and geometrical factors such as pore shape and interconnectivity. A straightforward use of the measured pore-size distribution will be used to determine an effective diffusivity. First, the relations for diffusion in a single cylindrical pore of diameter s will be summarized.

Two limiting cases are relevant to diffusion in pores of typical size range and when adsorbate concentration is small. When pore size is sufficiently large, collisions of the gas molecules with the pore wall are infrequent compared with collisions with other molecules, and the diffusivity approaches that in a free gas, ϑ. The Chapman Enskog dense gas theory (Hirschfelder et al., 1954) is then appropriate. The value determined for the conditions of the experiment is given in Table 1. When the pore size is sufficiently small, molecules rarely collide with each other and diffusion is determined by collision with the pore wall. The accepted relation given by Knudsen (1909) can be expressed as follows:

$$\vartheta_K = \frac{s}{3}\sqrt{\frac{8RT}{\pi M}}\,, \tag{13}$$

where R is the gas constant and M is the mean molecular mass of adsorbate molecules. The radical expression is the mean molecular velocity. One can see that the diffusivity increases with pore size in the Knudsen regime.

The usual relation for the combined diffusivity, ϑ_P, due to both Knudsen and free diffusion effects is

$$\vartheta_P = \left[\frac{1}{\vartheta} + \frac{1}{\vartheta_K}\right]^{-1}. \tag{14}$$

This relation produces the correct diffusivity in each of the two limits. Other transition relations are possible, for example, the exponential transition suggested by Wheeler (1951). An exponential transition produces a diffusivity for the intermediate pore sizes that is greater than that of Eq. 14 by up to 30%. Equation 14 with Eq. 13 is used here to represent the diffusivity for diffusion along a pore as a function of pore size, s. Account must now be taken of the distribution of pore sizes and of pore structure to determine the effective diffusivity, ϑ_e. The pore structure of the particles will be taken as uniform. For example, the porosity and the moments of the pore-size distribution of a given particle and for all particles will be considered uniform. A relatively simple relation is found under the further reasonable assumption that the pore passages are well connected to one another.

The diffusion flux in the direction of the mean composition gradient within the particle can be represented as the total diffusion flux due to pores of different sizes. With f_s the volume fraction distribution of pore size in the particle, the diffusion transfer rate in the radial direction of interest here can be expressed formally as

$$-\int_0^\infty \vartheta_P \frac{\partial \rho Y}{\partial r} f_s\, ds. \tag{15}$$

At any instant, the gradient of adsorbate density appearing in the integrand will depend on pore size. Representing the dependence of this gradient on pore size is complicated by the lack of information about connectivity of the pores. As a working approximation, it will be assumed that, at a given radial position, the gradient is independent of pore size. With this assumption, the diffusion transfer rate may be written as

$$-\overline{\vartheta}_P \frac{\partial \rho Y}{\partial r}, \tag{16}$$

where $\overline{\vartheta}_P$ is the mean pore diffusivity:

$$\overline{\vartheta}_P = \int_0^\infty \vartheta_P f_s\, ds, \tag{17}$$

with ϑ_P the function of s given by Eq. 14 with Eq. 13.

The preceding takes no account of the orientation of the pores, since it implicitly assumes all pores lie in the direction of the concentration gradient. As a result of pores that are orientated at an angle to the direction considered, the gradient will be correspondingly decreased by the factor $\cos\theta$, because the diffusion path length is increased by $1/\cos\theta$, where θ is the angle between the pore-axis direction and the gradient direction. Assuming all pore orientations for all pore sizes are equally probable, the mean pore diffusivity just given must be adjusted by the average of the factors for all orientations. Integrating the factor over area of the hemisphere on one side of the plane perpendicular to the gradient direction and dividing by the hemisphere area gives

$$\frac{1}{2\pi}\int_0^{\pi/2} 2\pi \cos\theta \sin\theta\, d\theta = \frac{1}{2}. \tag{18}$$

The inverse of this average factor is customarily termed the tortuosity factor, τ. The effective diffusivity is thus given by the relation

$$\vartheta_e = \frac{\overline{\vartheta_P}}{\tau} = \frac{1}{2}\int_0^\infty \vartheta_P f_s\, ds. \tag{19}$$

Provided that the pore size distribution is available, the effective diffusivity in the model is determined by these relations. For the measured pore-size distribution of the particles used in the experiment (Figure 3), ϑ_e is found to be 3.47×10^{-6} m^2/s (Table 1).

This method can be contrasted with a proposal of Wheeler (1951) in connection with the chemical reaction in porous catalysts and commonly cited in texts covering heterogeneous catalysis (Smith, 1981; Thomas and Thomas, 1997). In this approach, a single average pore size is used to determine pore diffusivity and other characteristics related to the pore structure. The average pore size that results is the diameter, s_{VS}, of a cylindrical pore having the same ratio of pore volume to pore surface area as the particle as a whole:

$$s_{VS} = 4\frac{V}{A} \tag{20}$$

in terms of the particle pore volume per mass, V, and pore surface area per mass, A. This representative pore size can be determined from the pore-size distribution, with the approximation that pores of a given size all have the same aspect ratio, to give

$$s_{VS} = \frac{1}{\int_0^\infty \frac{1}{s} f_s \, ds}. \tag{21}$$

With the factor $1/s$ proportional to the surface-area-to-volume ratio, this average pore size gives heavy weighting to the smallest pore sizes. From the measured volume distribution of pore size (Figure 3), s_{VS} is found to be 0.0058 μm for the particles used here. This pore diameter corresponds to a pore effective diffusivity of 2.17×10^{-7} m^2/s, that is, only about 6% of the value resulting from the volume mean of pore diffusivity proposed here.

The measured pore volume per mass, V, and the value of s_{VS} can be used to determine A from Eq. 20. This value should be comparable to the measured pore surface area per particle mass. This calculation gives $A = 743\times10^3$ m^2/kg, as compared to the BET surface area measurement of 717×10^3 m^2/kg (Table 1). The close agreement is somewhat surprising, as the two methods are not expected to agree precisely. The BET method makes no assumption about the pores being cylindrical, but contains uncertainty in the determination of the precise point of nitrogen adsorption corresponding to a monolayer of nitrogen over the entire pore surface.

Equilibrium Relation

The parameters in the Freundlich relation, Eq. 1, can reasonably be estimated using the Dubinin-Radushkevich (DR) theory, for example, Dubinin (1966). The theory uses the observation that adsorption is dominated by pores of size comparable to the adsorbate molecules, the micropores, and an assumed micropore-size distribution function to express the volume of condensed (adsorbed) adsorbate as a function of a micropore structure parameter, κ, a relative affinity coefficient, β, and the molar work of adsorption

$$A_W = RT \ln \frac{p_s}{p}, \tag{22}$$

where p is the partial pressure of adsorbate in the gas and p_S is the saturation vapor pressure of the adsorbate species. Taking the density of the condensed adsorbate to be the liquid density under standard conditions, $\rho_L = 1{,}600$ kg/m^3, the DR equilibrium relation can be written

$$m = \rho_L W_o \exp\left[-\kappa \left(A_W/\beta \right)^2 \right]. \tag{23}$$

The parameters in this relation can be determined for the present conditions following the procedure reported in Dubinin (1966) and Urano et al. (1982). The values found for the parameters in Eq. 23 are $W_o = 0.4\times10^{-3}$ m^3/kg, $\kappa = 1.8\times10^{-9}$ (mol/J)^2, and $\beta = 1.155$. The DR relation is not in the form of the Freundlich isotherm on which the modeling is based. Over the range of adsorbate concentration in the present experiment, the values $K = 985$ kg/m^3 and $q = 0.337$ give a representation of Eq. 23 to within about 1%.

Deviation from the DR theory is found for carbon materials having a relatively small fraction of pore volume in the micropores or possibly when the distribution of micropore sizes is unusual (Rodriguez-Reinoso and Linares-Solano, 1989). Also, the presence of secondary adsorbate species can affect adsorption of the primary adsorbate. The most likely secondary species is the water vapor present in the flue gas (about 5% by mass). At somewhat lower water-vapor concentrations than this and at ambient conditions, Werner (1985) found water vapor to have a significant effect on activated carbon adsorption of trichloroethylene, reducing the adsorbed trichloroethylene by up to more than 50% at low gas concentrations.

Residence Time

A final uncertainty in the comparison between the model and the experiment is associated with departures from the ideal of plug flow implicitly used in deriving the bulk conservation equations (Eqs. 10 and 11). There is reason to believe that significant three-dimensional effects occur in the particle injection region in the experiment. First of all, the injection jet is directed in the upstream direction and, thus, the injected gas and particles follow trajectories that must bend through 180° to proceed downstream. Also, there are four viewports just near the injection point that considerably alter the otherwise circular cross section of the pipe. While one could have solved the three-dimensional flow and particle conservation equations for the true geometry, together with the model equations for particle adsorption, it was felt that this considerable effort was not justified. Instead, an approximate study of the three-dimensional flow field produced in the vicinity of the viewports and injection was carried out to provide an estimate of the average residence time from injection through the three-dimensional region to the first measurement position at $x = 0.485$ m.

Commercial computational fluid-dynamics software (Fluent, 1996) was used to solve the governing equations for the turbulent particle-laden flow resulting from injection into the pipe flow. The geometry is approximated using a rectangular pipe section, although the main geometric relations, flow cross-sectional areas, and volumes are preserved. The solution domain in the vicinity of injection is shown in Figure 6, where it can be seen that advantage has been taken of the planar symmetry of the mean flow. The flow in the injector tube is included in the computation so that the skewing of the injection jet resulting from the sudden change in flow direction through the nozzle can be represented. The mean continuity, momentum, and k-ϵ turbulence model equations for the gas phase are solved together with stochastic Lagrangian equations for the particles (MacInnes and Bracco, 1991, 1992). Momentum coupling between the gas and particles is included. The grid used in the computations is $26\times91\times35$ cells, and average particle residence times are based on 25,000 sample particle trajectories, with particles released

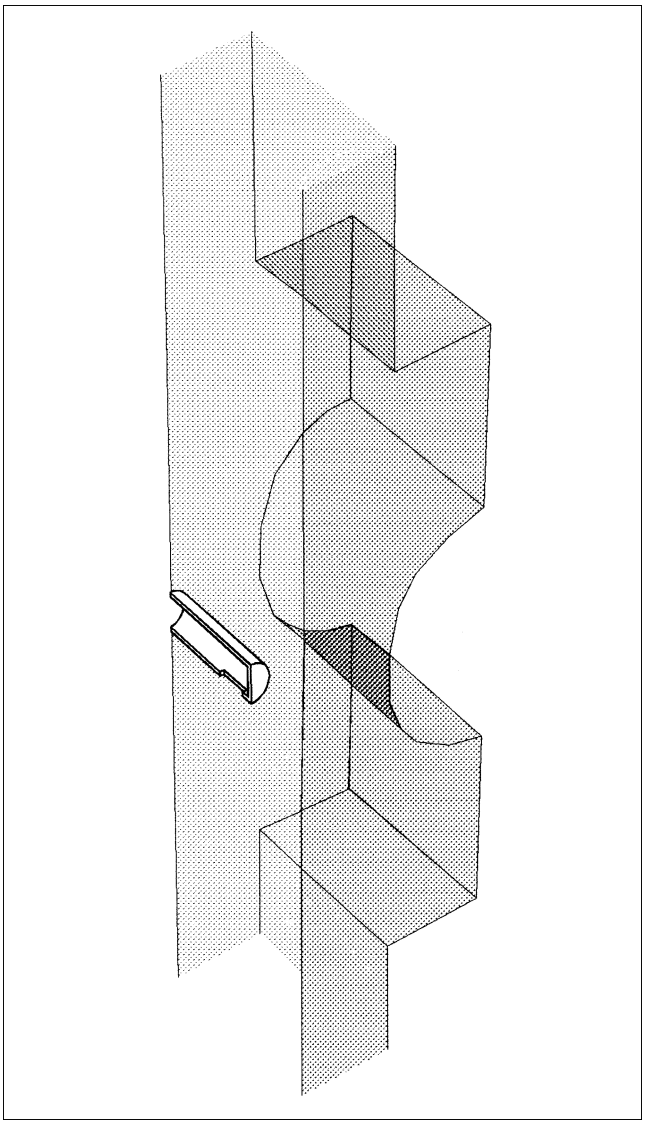

Figure 6. Three-dimensional flow computation domain in the vicinity of the particle and gas injection.

from five positions distributed over the injector tube inlet.

Figure 7 shows computed velocity vectors, particle trajectories, and adsorbate concentration, using two orthogonal views in the first two cases. The skewing of the injection jet is found to be significant. The particle trajectories shown indicate that the particles penetrate to about two pipe diameters upstream before turning back to travel in the main flow direction. The particles are more likely to be found on the side of the pipe to which the jet is skewed, although by the time the first measurement position is reached (5.9 pipe diameters downstream from the injection exit), they are uniformly distributed in the flow. The particles clearly find their way into the viewport volumes at the side of the pipe. One can see particles trapped in the viewport recirculation zones, particularly in the upstream viewport. It is noted that the bulk concentration is established rapidly following the introduction of the injection

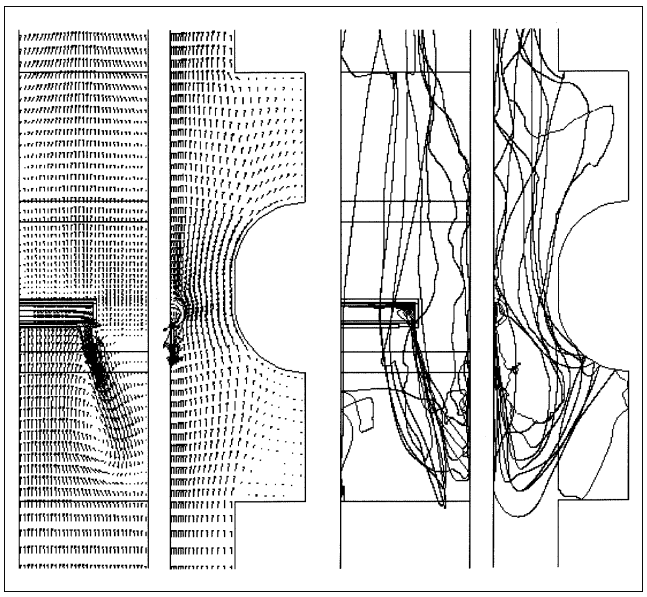

Figure 7. Computed character of the injection flow field with particles.

Views from two orthogonal directions of velocity vectors (in two planes passing through the injection nozzle) and sample particle trajectories.

air into the flue gas and adsorbate. After just one diameter, the gas reaches a composition that is uniform to within 3%.

Computations were made of a range of particle mass flow rates covering the experimental range. It was found that the average residence time varied somewhat with particle-mass loading. The computed residence times are shown in Figure 8 as a function of particle-mass loading (defined as the ratio of particle-mass flow rate and injection air-mass flow rate). The residence time is expressed as a ratio with the residence time $x/U = 0.0323$ s that would be found for plug flow in the pipe. The computation indicates a true residence time that is about twice the plug-flow residence time and that increases with particle-mass loading. One can easily understand the increasing residence time with mass loading in terms of the greater penetration upstream by a jet of greater momentum. Some of the increase may also result from changes in the flow field that allow more particles to find their way into the viewport recirculation zones.

The residence time is also found to depend on particle size. For an intermediate particle-mass flow rate, average residence time was determined for each of several particle sizes spanning the range of sizes in the distribution. The residence times determined are plotted after normalization by the average in Figure 9. There is a deviation by around $\pm 10\%$ of the average with the computations, indicating an increasing residence time with increasing particle size. While the computations indicate that residence time varies both with particle size and particle-mass flow rate, the residence time is generally about twice that for plug flow. In making comparisons with the experimental results, residence times for the experiment are determined using the computed average residence time to the first measurement position and the plug-flow residence time beyond the first measurement position.

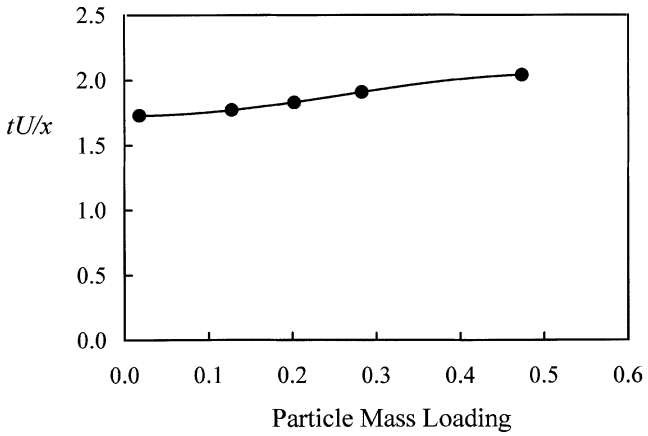

Figure 8. Computed influence of particle mass loading on average particle residence time in the flow from injection to the first measurement position.

Results

The model is now used to compute the change in bulk gas adsorbate mass fraction along the flow for the conditions of the experiments. The computation uses the parameter values estimated in the preceding sections, listed in Table 1, and the measured distribution of particle sizes (Figure 4). Mean residence times in the flow from injection to the three measurement positions in the experiment take account of the computed shift relative to plug flow associated with the complex injection flow field. The data for the adsorbate bulk mass-fraction measurements and the computed residence times to the first position downstream of injection are summarized in Table 3. These experimental results are compared in Figure 10 with the model computations, where the adsorbate "uptake", $1 - Y_B/Y_{Bo}$, is plotted as a function of time from injection.

The expected trends can be observed in the plot: uptake increasing both with time and with particle injection mass flow rate. A striking difference between the computation and the experiment is the overestimate of uptake by the model for

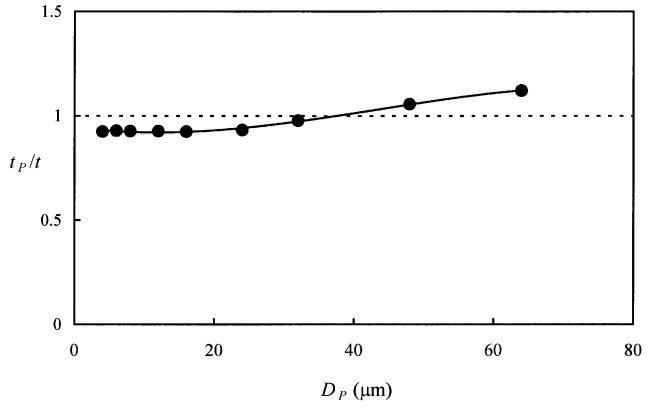

Figure 9. Dependence of mean residence time on the particle diameter.

Table 3. Measured Bulk Mass Fraction and Computed Average Residence Times to the First Measurement Position Downstream of Injection

	Avg. Residence Time to $x = 0.485$ m		Y_B/Y_{Bo}			
$\dot{M}$ (g/s)	$\frac{\tau_{0.485}U}{x_{0.485}}$	$\tau_{0.485}$ (ms)	$x = 0$	0.485 m	3.43 m	6.50 m
0.113	1.73	55.9	1.00	0.789	0.759	0.699
0.430	1.77	57.3	1.00	0.700	0.591	0.537
0.740	1.85	59.8	1.00	0.518	0.410	0.386
1.35	2.01	64.9	1.00	0.260	0.190	0.139

the three highest particle-mass flow rates. At the final measurement position where particles will have reached approximate equilibrium, this indicates inaccuracy in the equilibrium relation used in the computation. Since the overestimation of equilibrium occurs at the lowest bulk gas adsorbate concentrations, it is possible that effects of water vapor (Werner, 1985) are the cause. To explore the inaccuracy of the equilibrium relation, the Freundlich (DR) isotherm used in the computations was plotted with the equilibrium evidence that could be deduced approximately from the measurements. At the furthest measurement position downstream, diffusion of adsorbate will have progressed considerably into the particles so that the adsorbed mass will approximate that which would be in equilibrium with the bulk gas concentration. At the final measurement position, the nondimensional time, t^*, is 0.046 for a particle of the mean size. Results presented in Allen et al. (2001) indicate that approximately double this time would be required for the particles to be within a few percent of true equilibrium. Figure 11 gives a plot of the theoretical isotherm together with the four data points derived from the experiment. Even though the measured data are approximate, it is clear that the theoretical isotherm used is inadequate.

A second series of computations was made with an isotherm constructed to mimic the equilibrium behavior implied by the experiment. The isotherm data derived from the experiment

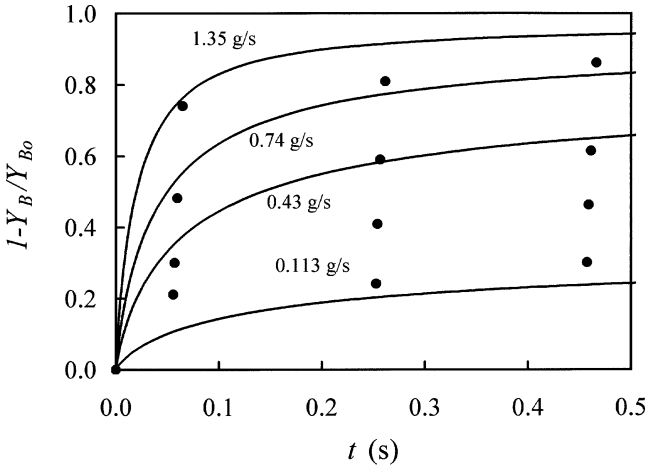

Figure 10. Comparison of the model of adsorbate uptake and that measured.

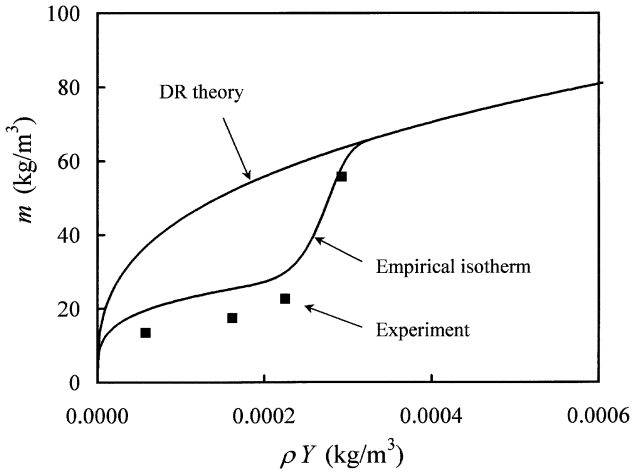

Figure 11. Theoretical and empirical isotherms compared with approximate equilibrium data of the experiment.

are expected to underestimate adsorbed mass at a given bulk gas concentration, since equilibrium has not been fully reached. Thus, the true isotherm will lie somewhat above the experimental points on Figure 11. On that figure is shown the constructed isotherm satisfying this rough constraint and which approaches the theoretical equilibrium relation at high adsorbate concentration. The effect of water vapor on the equilibrium curve found by Werner (1985) displays a similar behavior, with the adsorption being suppressed just at low adsorbate concentration by the presence of water vapor. The result of using this new isotherm in the model computation is shown, again with the experimental data, as the solid curves in Figure 12. The modification to the equilibrium relation brings the computation of the latter stages of adsorption into close agreement with the experiment. These results point to the importance of an accurate determination of the equilibrium relation for the actual conditions of interest.

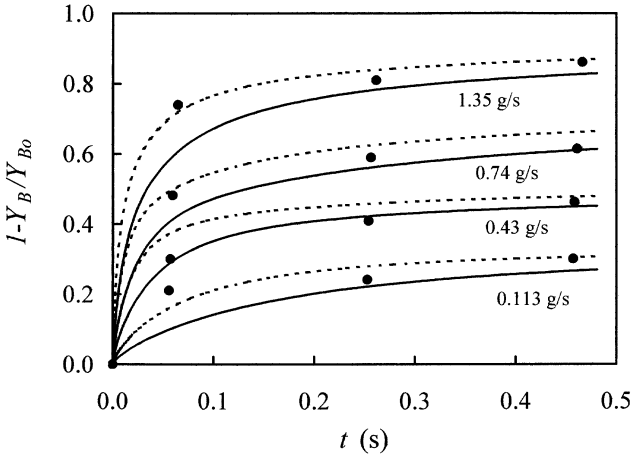

Figure 12. Model computation using empirical isotherm.

Solid curve with measured particle size distribution; dashed curve with particle size reduced to 0.68 of measured sizes.

One major difference remains. That is the underestimation of uptake by the model in the early stages of adsorption. At the first measurement position downstream of particle injection, the experiment shows consistently greater uptake than in the computation (i.e., the solid curves of Figure 12). The difference can be understood in terms of the time scale of the adsorption process given by Eq. 7. Since the model is reaching the correct equilibrium uptake, the adsorption rate in the model is too low. From Eq. 7 this means that the time scale $D_P^2(1+K^*)/\vartheta_e$ is too large, by about a factor of 2, according to the experimental result at the first position downstream. The possible problems in the model, therefore, are that the effective diffusivity within the particle is too low, K^* is too high, or the particle diameters are too large. Consideration of the uncertainties in the pore-size distribution, on which the diffusivities depend, led to an estimated error of at most about 10% in the diffusivity. Further, the diffusivity would be increased using the exponential function transition to the Knudsen regime in place of Eq. 14, as proposed by Wheeler (1951). The effect would move the computation in the direction of the experiment but only by a small fraction of the factor of 2 needed. The error in K^*, which depends on the equilibrium parameters and directly measured quantities, is estimated to be even smaller. Thus, inaccuracy in parameters involved in K^* or in the effective diffusivity cannot account for the slow adsorption given by the model.

One can note here also that determining the diffusivity using the average pore size proposed by Wheeler (1951) greatly worsens agreement. This average size is for a pore having the same volume-to-surface ratio as for all pores within the particles, and is given by Eq. 21. As mentioned in connection with that equation, the diffusivity determined in this way will be only 6% of that resulting from the present analysis, and that has produced the solid curves of Figure 12. A computation with the volume-to-surface pore size would give an adsorption rate of only about 3% of that indicated by the experiment.

The adsorption time scale is in fact most sensitive to the remaining parameter, the particle diameter, depending on its square. Smaller particle diameters than those represented by the measured distribution could account for the underestimation of adsorption rate. As mentioned earlier, the relation between actual particle shape and the diameter reported by the size measurement instrument is expected to be an overestimate of diffusion distance to the particle interior volume. For example, a particle in the shape of a cube has an average projected area of 1.5 times the area of one side of the cube, for equally probable orientation with respect to the projection direction. The size reported in the measurement for this particle for this average projected area is 1.38 times the cube side length, being the diameter of the sphere having the same projected area. For a particle in the shape of two cubes joined together at a side (a prism of square section and aspect ratio 2) the average projected area is 2 times the area of one side of the cubes and the reported size is 1.59 times the cube side length. The diameter, D_P, entering the model represents diffusion distance to the core of the particle. For the spherical particles assumed in the model this is the diameter of the sphere, but for a rectangular shape such as a cube the diffusion distance will be to that of the minimum side length. Reducing the particle sizes in the computation to account roughly for actual particle shape produces the results shown

with a dashed curve in Figure 12. The particle sizes in the measured distribution have been reduced by a factor midway between the cube side to projected area diameter values for the single and double cubes (a factor of 0.68). The shift in adsorption time scale due to this account of particle shape is about the right magnitude to account for the measurements. This result gives a clear indication of the need to improve the characterization of particle shape.

Conclusion

Measurements of adsorbate uptake by activated carbon particles are combined with a theoretical model to establish the adequacy of the modeling and clarify the critical parameters determining the adsorption. The conditions of the experiment correspond to those typical of dry sorbent injection which is used in cleaning gas streams. Particle-size and pore-size distributions are measured in the experiment to allow determination of the particle properties required in the model representation. Measurements of bulk gas adsorbate concentration at several positions downstream from particle injection are made to characterize adsorbate uptake by the particles.

The model used is that described in Allen et al. (2001), although considerable further development is made in relation to determining the particle parameters required by the model. A consistent treatment of intraparticle diffusivity is developed based on standard measured pore-size distribution. From the hypothesis of random pore channel distribution, a theoretical tortuosity factor of 2 is found to apply. The proposal of Wheeler (1951), which continues to be presented in texts without qualification, that the intraparticle diffusivity be determined as the diffusivity of the pore size having the same pore-volume-to-pore-surface-area ratio as the particle as a whole, is shown to greatly underestimate pore diffusion for the activated carbon considered.

The equations are integrated in time along the flow as the gas and particles travel downstream from the particle injection position. The complexity of the particle injection flow field, which involves injection in the upstream direction and recirculation zones in adjacent view port volumes, prompted an estimation of mean residence time for particles moving through this injection region. Three-dimensional computations of the flow with particle injection were made to establish mean residence time and its dependence on particle size and particle-mass loading. The residence times determined were used for the time from injection to each downstream position in the experiment.

The Dubinin-Radushkevich equilibrium relation is initially applied in the modeling. This leads to a poor account of the experiment results. It is found that the measurements at the furthest downstream positions, which are in approximate equilibrium, give an indication that adsorption at low adsorbate concentration is lower than that given by the theoretical equilibrium relation. Evidence from other work suggests this may be the result of the presence of water vapor in the gas. Use of an empirical equilibrium curve to fit the equilibrium points implied by the downstream measurements, yet consistent with the theoretical relation at large adsorbate concentrations, produces good agreement with the downstream measurements.

Comparison of the model with the measurements from injection along the length of the flow indicates the adsorption time scale produced by the model to be about double that implied by the experiment. Consideration of the possible weaknesses in the model suggests that misrepresentation of particle size when the measured size distribution is used directly is the most likely cause. Were the experimental particles all spherical in shape (an assumption both of the model and the size measurement technique), the model would be expected to agree with measurement, although this remains to be proven. It is argued that nonspherical particle shape causes an overestimate of particle effective diffusion length resulting from the size measurement. The degree of the effect is demonstrated by an approximate adjustment of the size distribution to account for particle shape.

Literature Cited

Allen, R. W. K., E. D. Archer, and J. M. MacInnes, "Adsorption by Particles Injected into a Gas Stream," *Chem. Eng. J.*, **83**, 165 (2001).

Archer, E. D., "The Removal of Volatile Organic Compounds from Combustion Flue Gases by Activated Carbon Adsorbents," PhD Thesis, Univ. of Sheffield, Sheffield, UK (2000).

Dubinin, M. M., "Porous Structure and Adsorption Properties of Active Carbons," *Chemistry and Physics of Carbon*, Vol. 2, P. L. Walker, ed., p. 51 (1966).

Fluent, *User's Guide, Version 4.4*, Fluent Incorporated, Lebanon, New Hampshire (1996).

Hirschfelder, J. O., C. F. Curtiss, and R. B. Bird, *The Molecular Theory of Gases and Liquids,* Wiley, New York (1954).

Kaye, B. H., *Characterization of Powders and Aerosols*, Wiley-VCH, New York (1999).

Knudsen, M., *Ann Physik*, 29, 179 (1909).

Lin, T.-F., J. C. Little, and W. W. Nazaroff, "Transport and Sorption of Organic Gases in Activated Carbon," *J. Environ. Eng.*, 169 (1996).

MacInnes, J. M., and F. V. Bracco, "Stochastic Particle Dispersion Modeling and the Tracer-Particle Limit," *Phys. Fluids A*, **4**, 2809 (1992).

MacInnes, J. M., and F. V. Bracco, "Comparisons of Deterministic and Stochastic Computations of Drop Collisions in Dense Sprays," *Numerical Approaches to Combustion Modeling,* E. S. Oran and J. P. Boris, eds., *Progress in Astronautics and Aeronautics*, Vol. 135, p. 615 (1991).

Rizk, M. A., and S. E. Elghobashi, "A Two-Equation Turbulence Model for Dispersed Dilute Confined Two-Phase Flows," *Int. J. Multiphase Flow*, **15**, 119 (1989).

Rodriguez-Reinoso, F., and A. Linares-Solano, "Microporous Structure of Activated Carbons as Revealed by Adsorption Methods," *Chemistry and Physics of Carbon*, Vol. 21, P. A. Thrower, ed., p. 1, (1989).

Smith, J. M., *Chemical Engineering Kinetics*, 3rd ed., McGraw-Hill, New York (1981).

Thomas, J. M. and W. J. Thomas, *Principles and Practice of Heterogeneous Catalysis*, VCH, New York (1996).

Urano, K., S. Omori, and E. Yamamoto, "Prediction Method for Adsorption Capacities of Commercial Activated Carbons in Removal of Organic Vapors," *Environ. Sci. Technol.*, **16**, 10 (1982).

Werner, M. D., "The Effects of Relative Humidity on the Vapor Phase Adsorption of Trichloroethylene by Activated Carbon," *Amer. Ind. Hyg. Assoc. J.*, **46**, 585 (1985).

Wheeler, A., "Reaction Rates and Selectivity in Catalyst Pores," *Advances in Catalysis*, Vol. 3, W. G. Frankenburg, V. I. Komarewsky, E. K. Rideal, P. H. Emmett, and H. S. Taylor, eds., p. 249 (1951).

Manuscript received Oct. 18, 2000, and revision received May 17, 2001.